Materials Today: Proceedings xxx (xxxx) xxx

Contents lists available at ScienceDirect

Materials Today: Proceedings

journal homepage: www.elsevier.com/locate/matpr

Experimental modal analysis of a cross-laminated timber slab

M. Kawrza [a], T. Furtmüller [a], C. Adam [a,*], R. Maderebner [b]

[a] University of Innsbruck, Unit of Applied Mechanics, Technikerstr. 13, Innsbruck, Austria
[b] University of Innsbruck, Unit of Timber Engineering, Technikerstr. 13, Innsbruck, Austria

ARTICLE INFO

Article history:
Received 16 November 2021
Received in revised form 2 February 2022
Accepted 12 April 2022
Available online xxxx

Keywords:
CLT
Experimental modal analysis
Complex mode shapes
Modal parameter estimation

ABSTRACT

This paper presents the results of an investigation of the dynamic response of a point-supported cross-laminated timber (CLT) slab without joists with a column grid of 5.0 × 5.0 m and overall dimensions of 16.0 × 11.0 × 0.2 m. The results are based on a detailed experimental modal analysis, identifying seven modes from the dynamic response of 651 measurement points, including natural frequencies, mode shapes and damping ratios. These modal parameters exhibit a time variance that is due to environmental influences during the measurement period of two days. As a result of this disturbance effect, the determined mode shapes have a non-negligible imaginary part, which is eliminated by correcting each of the 73 measurements individually. The findings presented provide in-depth insight into the dynamic behavior of the large-scale CLT structure with point supports realized with a novel steel connector.

1. Introduction

As a serious alternative to concrete and masonry structures, timber structures have gained importance both for single-story and multi-story buildings, especially since the development of cross-laminated timber (CLT). CLT is a panel composed usually of 3, 5 or 7 layers of lamellas glued together on their side faces, with the adjacent layers aligned perpendicular to each other [1,2]. From an economic point of view, flat slabs without joists have the advantage that the total height of the floor structure can be reduced considerably compared to structures with joists, although thicker CLT panels have to be used. One of the first multi-story buildings constructed with point-supported flat slabs without joists is the 18-story tall mass timber hybrid student residence at the University of British Columbia in Vancouver [3]. In this building, the point supports are located at the corners and edges of each panel, which results in a rather narrow column grid of 2.85 × 4.0 m. However, to extend the application range, the span width must be considerably increased. These larger spans can be achieved for point-supported flat slabs without joists by means of a new type of support system with a steel connector [4,5], which also allows to build timber structures with spans of up to seven meters.

Compared to, for example reinforced concrete, timber structures have a high stiffness-to-weight ratio, which allows the construction of comparatively lightweight structures. On the other hand, this makes timber structures more prone to vibrations, therefore serviceability must be carefully checked during the design process. In floor structures, these vibrations are mainly caused by the occupants walking or jumping, or by falling objects. They can lead to severe discomfort for the occupants if the natural frequencies of the human body are excited [6]. This is especially true for the low frequency range. At higher frequencies, the vibrations can lead to annoyance due to structure-borne noise. To ensure serviceability, a number of studies have been carried out on the dynamic response of timber floor systems under laboratory and in-situ conditions [7–10].

In the present contribution, the dynamic behavior of a point-supported flat slab without joists, realized with the aforementioned novel steel connector, is investigated. In contrast to previous studies, a detailed experimental modal analysis is performed to identify a number of natural frequencies, corresponding modal damping ratios and mode shapes. The goal of this study is (*i*) to gain insight into the dynamic behavior of a large-scale structure with novel steel connectors and (*ii*) determine the influence of the boundary conditions on the slab dynamics.

2. Test specimen

The object under investigation is a 16.0 m × 11.0 m × 0.2 m point-supported flat slab composed of seven cross-laminated-timber (CLT) panels with widths between 1.75 m (edge panels)

* Corresponding author.
E-mail address: christoph.adam@uibk.ac.at (C. Adam).

https://doi.org/10.1016/j.matpr.2022.04.559

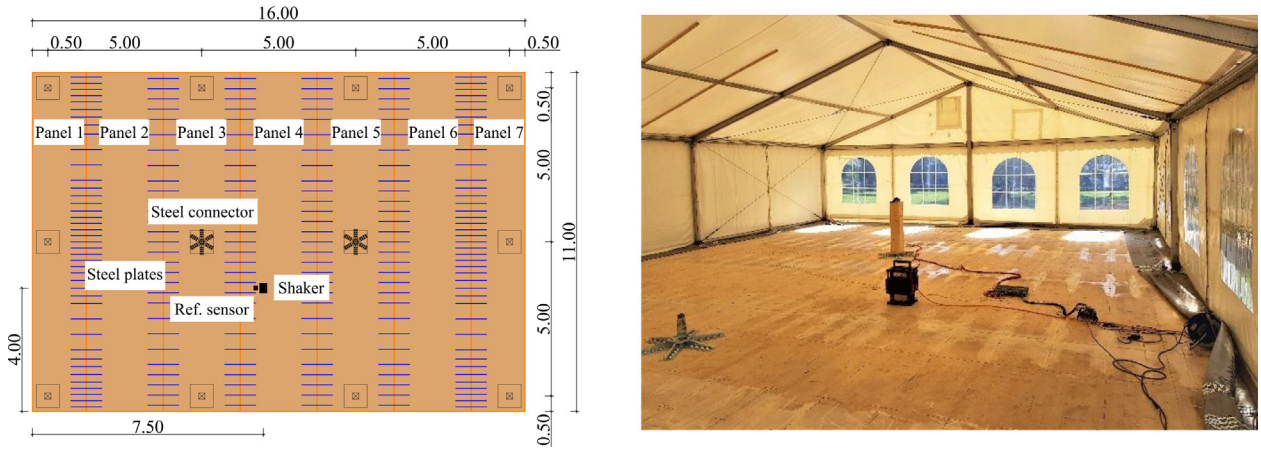

Fig. 1. Floor plan of the test object (left), photo of the test object with test setup (right).

and 2.5 m (inner panels), see Fig. 1. The CLT panels consist of seven layers of spruce lamellas glued perpendicular to each other. The individual layers each have a thickness of 2-4-2-4-2-4-2 cm, with the top layer aligned parallel to the longitudinal direction of the slab. The panels are connected with a total 196 steel plates cast in epoxy resin with overall dimensions of 80 cm × 18 cm × 0.5 c m, with the distribution of the plates within the six panel joints depicted in Fig. 1. The slab is supported by 12 columns with a grid of 5.0 m × 5.0 m. The two inner supports are reinforced with a star-shaped steel connecter. The timber columns made ofspruce and a cross-section of 0.2 m × 0.2 m are fixed to prefabricated concrete foundations with dimensions of 0.75 m × 0.75 m × 0.5 m. As can be seen in Fig. 1, the object is protected with a tent construction. The aluminum columns of the tent are directly attached to the top of the 10 outer columns supporting the slab, therefore the influence of the tent on the dynamic properties is assumed to be negligible.

3. Methods

3.1. Experimental modal analysis

The test object was excited with the reaction masses, type APS 0412, of an electrodynamic long-stroke oscillator, type APS 400, driven by a power amplifier, type APS 145. In total this setup consists of 35 kg of dynamically active mass and 70 kg of static mass fixed at a defined position (cf. Fig. 1). To compensate for resonance effects, the input signal, which consists of a linear sweep with an initial signal ramp and an end signal decay period of 10 s each, was adjusted such that the frequencies in the considered range were excited evenly. Therefore, prior to the measurements an iterative adjustment of the voltage input signal was necessary until the power spectral density of the excitation accelerations at the oscillating reaction masses was constant in the defined frequency range. For these measurements, the linear sweep from 6 Hz to 50 Hz was performed four times in succession for 120 s. The dynamic response (output) was recorded at 651 measuring points on the surface of the CLT slab with piezoelectric accelerometers type Brüel&Kjær 4508B powered by a conditioning amplifier type Brüel&Kjær 2694. Additionally, a reference sensor type Brüel&Kjær 8344 recorded the output next to the shaker during the measurements. A National Instruments (NI) cDAQ module with NI 9234 A/D converters was used for data acquisition, controlled by a MATLAB program. The measurement points were arranged in a rectangular grid with a spacing of 0.5 m between the points in longitudinal and transverse directions (cf. Fig. 2). The dense grid was

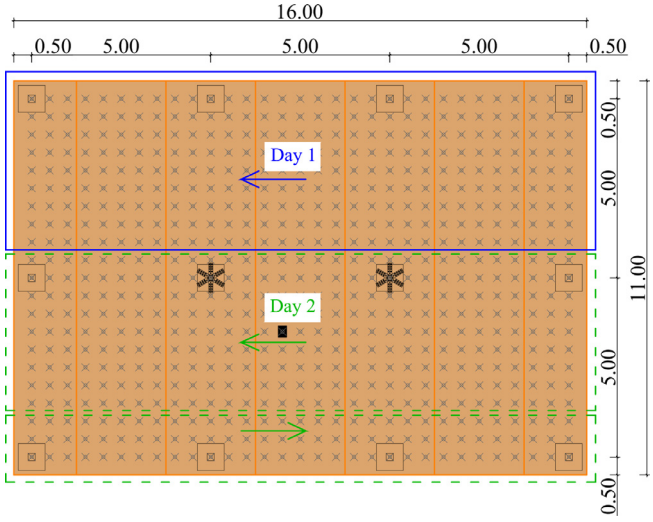

Fig. 2. Measurement points and direction of the 31 measurements on day 1 and direction of the 42 measurements on day 2.

chosen to be able to identify any local effects in the mode shapes due to the point supports or the joints. Nine accelerometers were available for the experimental modal analysis, resulting in a total of 73 individual measurements to capture the dynamic response of the entire slab. On the first day, 31 measurements were made, recording the response of the upper half of the slab, which is highlighted in Fig. 2 by a rectangular frame with solid lines. The direction of the measurements from the right side to the left side is indicated with an arrow. On the second day, the dynamic response of the lower half of the slab was recorded with a total of 42 measurements, where the first 31 measurements were identically to the first day and the dynamic response of the remaining points was recorded with 11 measurements from the left side to the right side at the bottom of the slab (highlighted with rectangular frames with dashed lines). Considering the length of individual sweep signals, a total of almost 10 h was required to carry out the measurements. Including the work to rearrange the sensors, two days were needed to complete the measurements.

4. Results

4.1. Modal parameter estimation (MPE)

For the estimation of the modal parameters (natural frequencies, mode shapes and damping ratios) from the experimentally

obtained frequency response functions (FRFs) of this single input multiple output system [11], the least squares complex frequency (LSCF) method [12] is chosen, which yields the stabilization diagram [13] shown in Fig. 3 in the frequency range from 6 to 50 Hz and model orders between 15 and 50. The counterpart of the LSCF method to identify the poles of the system in the time domain is the least squares complex exponential (LSCE) method [11]. The main difference between these two methods is that the LSCE method determines the polynomial coefficients to estimate the poles from the impuls responses, while the LSCF method uses the frequency response functions. The result of the estimated poles of these two methods is expected to be equivalent. However, one advantage of the LSCF method over the LSCE method is the very clear stabilisation diagrams that makes it easier to distinguish between physical and mathematical poles. An explanation of the clearer stabilization diagrams and the algorithm of the LSCF method can be found in [14]. The poles in the stabilization diagram are considered stable (P_{st}) if the relative changes in the i-th natural frequency Δf_i^{EMA} and the i-th damping ratio $\Delta\zeta_i$ between two model orders m-1 and m are within the following values,

$$\Delta f_i^{\text{EMA}} = \frac{\left| f_{i(m-1)}^{\text{EMA}} - f_{i(m)}^{\text{EMA}} \right|}{f_{i(m-1)}^{\text{EMA}}} 100 \leq 1\% \tag{1}$$

$$\Delta\zeta_i = \frac{\left| \zeta_{i(m-1)} - \zeta_{i(m)} \right|}{\zeta_{i(m-1)}} 100 \leq 10\% \tag{2}$$

Otherwise, if the relative changes in natural frequencies or damping ratios are not met, the pole is identified as new, which is denoted as P_{new} in the figure. For the mode to be considered as stable ($Mode_{st}$), additionally the criterion.

$$\Delta\phi_i = \text{MAC}\left(\text{Re}\left(\{\phi\}_{i(m-1)}\right), \text{Re}\left(\{\phi\}_{i(m)}\right)\right) \geq 0.95 \tag{3}$$

must be met, where the difference $\Delta\phi_i$ between the real parts of the i-th mode shape vector $\text{Re}\{\phi\}_i$ between to model orders is evaluated using the modal assurance criterion (MAC) [15].

The identified poles and modes are depicted in Fig. 3, where circular markers indicate stable modes, cross-shaped markers indicate stable poles and dots indicate new poles. Additionally, the mean of all 651 computed FRFs is shown by a solid line to visually identify the physical poles.

According to the modal parameter estimation procedure, the fundamental frequency of the tested structure is found to be 10.51 Hz. The stabilization diagram indicates a number of stable poles for higher modes, but after visual inspection of the mode shapes, a total of seven modes are considered stable in this frequency range. The identified natural frequencies f_i^{EMA} and damping ratios ζ_i are listed in Table 1. The natural frequencies for higher modes identified are between 11.49 Hz and 31.69 Hz with corresponding damping ratios between 1.25 and 3.23 %. It should be noted that the subscript i in Table 1 indicates the identified mode and not necessarily the actual mode of vibration of this structure.

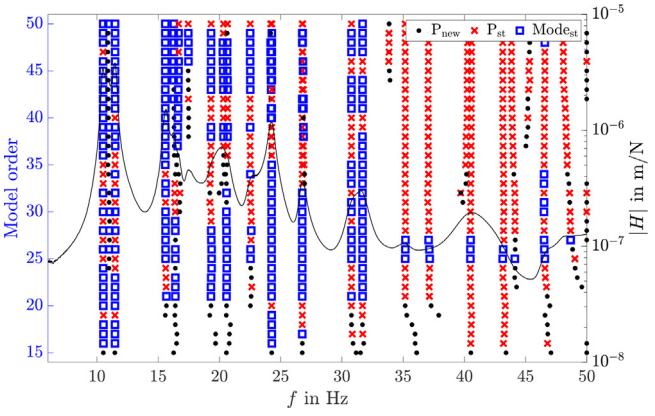

Fig. 3. Stabilization diagram of the point supported slab resulting from the MPE.

The real parts of the corresponding modal displacements corrected with the central axis rotation, which is described in Appendix A, are depicted in Fig. 4. The fundamental mode $\{\phi\}_1$ is a bending mode with a distinct nodal line in the longitudinal direction. Although the geometry of the structure is completely symmetric, the identified mode shape shows a relatively strong longitudinal asymmetry with larger modal amplitudes in the right part of the slab. The largest modal amplitudes for the second mode shape $\{\phi\}_2$ are in the area of the shaker position, suggesting that the second mode is a result of the structure interacting with the shaker [16], which in itself is a vibrating system. As the natural frequency increases, the asymmetry in the mode shapes $\{\phi\}_3$ to $\{\phi\}_7$ decreases and mode shapes with nodal lines in the longitudinal und transverse directions are obtained.

4.2. Complex mode shapes

Due to the MPE method, the components of the mode shape are in general complex. The imaginary part of the mode shapes can usually be neglected for lightly damped systems, as in this case. To quantify the contribution of the imaginary part on the mode shape, the mean phase correlation (MPC) is used, which is defined as [17].

$$\text{MPC}_i = 1 - \frac{||\text{Im}(\{\phi\}_i)||}{||\text{Re}(\{\phi\}_i)||} \tag{4}$$

where $\text{Im}(\{\phi\}_i)$ is the imaginary part of the mode shape vector $\{\phi\}_i$ and $\text{Re}(\{\phi\}_i)$ is the real part. If the MPC value is close to unity, then the mode shape is a real mode, but if the MPC value is close to zero, the mode shape is complex. Note that the mode shape vector components, which should be colinear in the complex plane, must be rotated so that they are aligned with the real axis before evaluating Eq. (4). The MPC values for the identified modes $\text{MPC}_i^{(0)}$ are between 0.74 and 0.89 (cf. third column of Table 1), and therefore have a rather large imaginary component, which contradicts with the theory.

During the measurements, a stationary reference sensor was placed next to the shaker, which is depicted in Fig. 1. In Fig. 5, the 73 FRFs of the reference sensor are compiled in a spectrogram for the frequency range between 10 and 11 Hz, i.e. close to the identified fundamental frequency, as a function of the recording time. The maximum of the spectrogram corresponds to the first natural frequency. On the first day, the measurements were recorded between 11:00 am and 6:30 pm and on the second day between 9:00 am and 5:30 pm. During the measurements of the first day, a slight decrease in the fundamental frequency is

Table 1
Experimentally identified natural frequencies and damping ratios and computed MPC values before and after correction.

Mode (i)	f_i^{EMA}[Hz]	ζ_i [%]	$\text{MPC}_i^{(0)}$	$\text{MPC}_i^{(c)}$
1	10.51	3.23	0.81	0.95
2	11.49	2.22	0.86	0.96
3	15.60	1.66	0.88	0.96
4	22.52	2.57	0.89	0.93
5	24.26	1.50	0.87	0.96
6	26.76	1.25	0.86	0.94
7	31.69	2.00	0.74	0.87

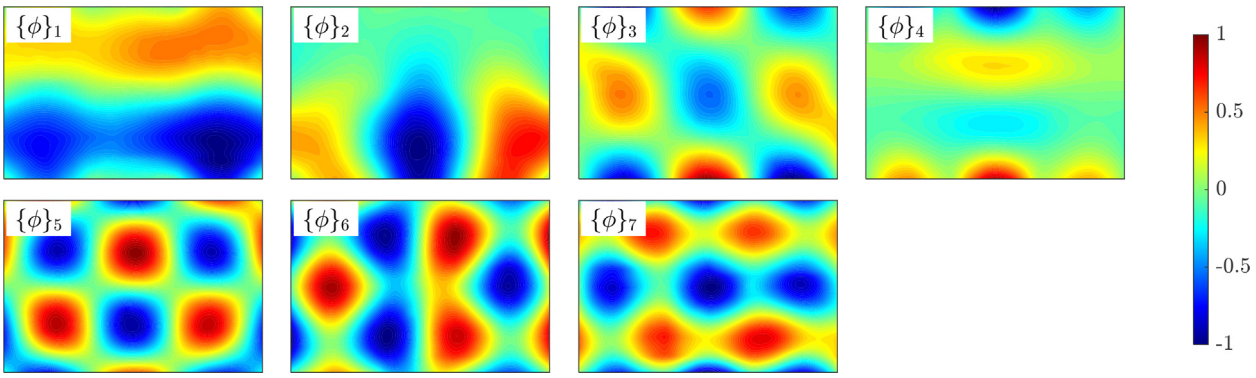

Fig. 4. Corrected mode shapes 1 to 7.

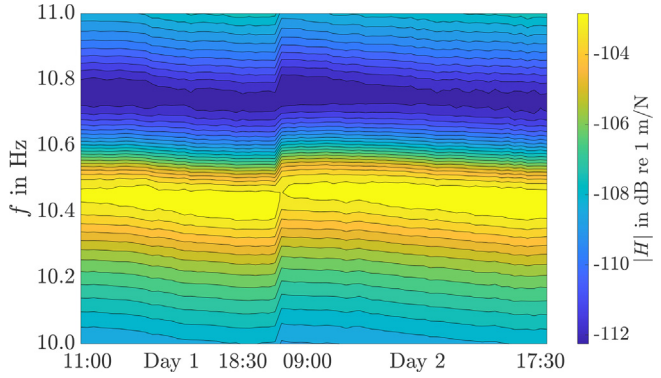

Fig. 5. Spectrogram near the fundamental frequency with time of each measurement [18].

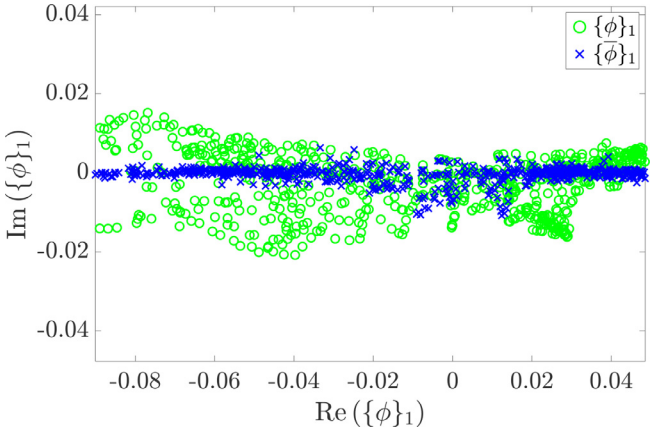

Fig. 6. Scatter plot of the components of mode 1 before and after correction [18].

observed, during the night, when no measurements were recorded, the natural frequency increases and during the second day a decrease is again observed. It is assumed that this behavior is due to fact that the soil stiffness (and thus the stiffness of the supports) changes during the course of a day due to solar radiation, as the CLT slab was erected on a meadow for demonstration purposes. A condition of modal analysis is that the system measured must be a linear time-invariant (LTI) system, which is thus violated. Therefore, strictly speaking, the tested structure is a time-varying system, which means that the natural frequencies and damping ratios listed in Table 1 are mean values of the time-varying modal parameters of the slab. The mode shapes in the MPE procedure are determined after the poles of the system have been identified, and consequently the identified mean poles lead to complex mode shapes. In order to minimize the imaginary part in the mode shape vectors, the 73 measurements are treated independently and subsequently corrected by central axis rotation (CAR) [17], which is described in Appendix A.

Therefore, the i-th mode shape vector $\{\phi\}_i$ is divided into individual subsets $\{\varphi\}_i^{(k)}$, with k = 1,2, …, 73. For each subset an individual central axis rotation angle $\delta_i^{(k)}$ is computed. In Fig. 6 the result of the piecewise rotation is illustrated, where the 651 components of the fundamental mode shape vector $\{\phi\}_1$ (circular markers) and the modified mode shape vector $\left\{\bar{\phi}\right\}_1$ (cross-shaped markers) are depicted. As can be seen, the correction significantly reduces the imaginary part of the components and the modified vector can be regarded real, as suggested by the relatively low damping values of the system. The improvement of this piecewise rotation is also evident in Table 1, where the $\mathrm{MPC}_1^{(c)}$ value of the modified first mode shape vector is 0.95, in contrast to the $\mathrm{MPC}_1^{(0)}$ value of the original vector with 0.81. In general, the $\mathrm{MPC}_i^{(c)}$ values of the modified mode shape vectors are all between 0.87 and 0.96, while the original $\mathrm{MPC}_i^{(0)}$ values are all lower than 0.9.

The left plot in Fig. 7 shows the correction angles $\delta_i^{(k)}$ normalized by the median of each function for the first three mode shapes. The dashed curves with circular, plus-shaped and asterisk markers illustrate the correction angles for the first, second and third mode, respectively, over the number of measurements on day 1 (measurements 1–32) and day 2 (measurements 33–74). In addition, the ambient temperature recorded during each measurement is depicted as a solid curve. During the two days of recording, the ambient temperature was between 13 and 21 °C. The right plot of Fig. 7 shows the correction angles $\delta_i^{(k)}$, also normalized by the median of each function for the last four modes identified. In this plot, dashed curves with dots, cross-shaped, triangle-shaped and squared markers illustrate the correction angles for the fourth, fifth, sixth and seventh mode, respectively, over the number of measurements. As discussed above, the system is time-varying, which is probably due to environmental influences. Since the boundary conditions generally have a significant impact on the lower natural frequencies, as can be seen in Fig. 4, where a stronger asymmetry in the lower modes is observed, a close correlation with the ambient temperature is also observed for the angles of the first mode shape. For the other identified mode shapes, however, the correlation is not as pronounced, as can be seen, for example, in the third and fourth mode.

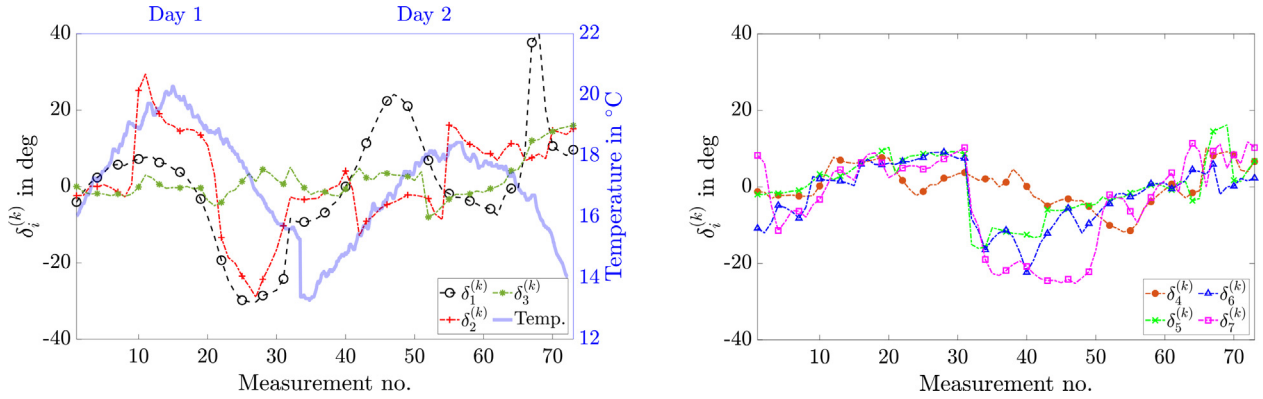

Fig. 7. Ambient temperature, correction angles for first three mode shapes. i = 1, 2, 3 (left); correction angles for the fourth to seventh mode shape, i = 4,5,6,7 (right).

5. Conclusion

In this contribution, the dynamic properties of a point-supported flat slab without joists composed of seven cross-laminated timber (CLT) panels were investigated experimentally. Based on the dynamic response of 651 measuring points, a detailed experimental modal analysis in the low frequency range was performed. The fundamental mode with a corresponding natural frequency of 10.51 Hz as well as six higher modes could be identified for this wide span panel with a column grid of 5.0 m × 5.0 m and overall dimensions of 16.0 m × 11.0 × 0.2 m. As these spans are only possible in timber engineering with novel star-shaped steel connectors used, they are expected to extend the application range of CLT. The modal properties determined from the experimental data recorded two days, exhibited a time-variance that violated the conditions of modal analysis. This disturbance effect is attributed to environmental influences that led to unexpectedly high imaginary parts in the mode shape vectors. However, this disturbance could be successfully corrected by a central axis rotation of the mode shape vectors by considering each measurement individually. This paper provides insights into the dynamic response of long-span CLT structures with this novel support system.

CRediT authorship contribution statement

M. Kawrza: Investigation, Methodology, Software, Formal analysis, Writing – original draft. **T. Furtmüller:** Conceptualization, Methodology, Investigation. **C. Adam:** Conceptualization, Resources, Supervision, Writing – review & editing. **R. Maderebner:** Resources, Conceptualization.

Declaration of Competing Interest

The authors declare that they have no known competing financial interests or personal relationships that could have appeared to influence the work reported in this paper.

Appendix A. Central axis rotation (CAR)

Identifying the mode shape vectors with modal parameter estimation methods yields complex values for the vector components. Although the phase angle is arbitrary, the predominant information of the mode shape is aligned with the real axis and therefore the imaginary parts of the vector must be minimized, specifically the central axis angle [17] must be minimized.

In the first step, a singular value decomposition (svd) of the relationship between the real part, $\mathrm{Re}(\{\phi\}_i)$, and the imaginary part, $\mathrm{Im}(\{\phi\}_i)$, of the i-th mode shape vector $\{\phi\}_i$ is performed, yielding the matrix $[V]$ [17],

$$[U,\Sigma,V] = \mathrm{svd}\left(\left[\mathrm{Im}\left(\left\{\phi\right\}_i\right)\mathrm{Re}\left(\left\{\phi\right\}_i\right)\right]^T\left[\mathrm{Im}\left(\left\{\phi\right\}_i\right)\mathrm{Re}\left(\left\{\phi\right\}_i\right)\right]\right) \tag{A.1}$$

Note that the right singular vector matrix is always a two by two matrix regardless the number of vector components. Then, the i-th central axis angle δ_i is evaluated using the four-quadrant inverse tangent of the right singular vector relationship [17],

$$\delta_i = tan^{-1}\left(-\frac{V_{22}}{V_{12}}\right) \tag{A.2}$$

In the last step, the imaginary parts are minimized by rotating the vector $\{\phi\}_i$ according to.

$$\left\{\bar{\phi}\right\}_i = \{\phi\}_i exp(-j\delta_i) \tag{A.3}$$

which yields the modified mode shape vector $\left\{\bar{\phi}\right\}_i$ [17]. In Eq. (A.3) j denotes the imaginary unit.

References

[1] R. Brandner, G. Flatscher, A. Ringhofer, G. Schickhofer, A. Thiel, Cross laminated timber (CLT): overview and development, Eur. J. Wood Prod. 74 (3) (2016) 331–351.
[2] BSPhandbuch: Holz- Massivbauweise in Brettsperrholz; Nachweise auf Basis des neuen europäischen Normenkonzepts [CLT handbook: Solid wood construction in cross laminated timber; Verifications based on the new European standards], 2nd ed., Publisher TU Graz (in German), 2010.
[3] P. Fast, B. Gafner, R. Jackson, J. Li, Case study: an 18 storey tall mass timber hybrid student residence at the University of British Columbia, Vancouver, Proc. 14th World Conference on Timber Engineering (WCTE2016), Vienna, Austria, 2016.
[4] B. Maurer, R. Maderebner, P. Zingerle, I. Färberböck, M. Flach, Point-supported flat slabs with CLT panels, Proc. 15th World Conference on Timber Engineering (WCTE2018), Seoul, Korea, 2018.
[5] R. Maderebner, Connecting device for mounting a wooden construction element, Patent US20180371741 (A1), 2018-12-27.
[6] H.E. von Gierke, A.J. Brammer, Harris' shock and vibration handbook - Effects of shock and vibration on humans, McGraw-Hill, New York, 2010.
[7] P. Hamm, A. Richter, S. Winter, Floor vibrations-new results, Proc. 11th World Conference on Timber Engineering (WCTE2010), Riva del Garda, Italy, 2010.
[8] H. Kreuzinger, B. Mohr, Gebrauchstauglichkeit von Wohnungsdecken aus Holz: Abschlußbericht [Serviceability of wooden floors: Final report], Fraunhofer-IRB-Verlag (in German), 1999.
[9] J. Weckendorf, E. Ussher, I. Smith, Dynamic response of CLT plate systems in the context of timber and hybrid construction, Compos. Struct. 157 (2016) 412–423.
[10] K. Jarnerö, A. Brandt, A. Olsson, Vibration properties of a timber floor assessed in laboratory and during construction, Eng. Struct. 82 (2015) 44–54.
[11] D.J. Ewins, Modal testing: Theory, practice and application, second. ed., Research Studies Press, Baldock, 2000.

[12] P. Verboven, Frequency-domain system identification for modal analysis, Ph.D. thesis (2002).
[13] W. Heylen, S. Lammens, P. Sas, Modal analysis theory and testing, Katholieke Univ. Leuven Dep. Werktuigkunde, Heverlee, Belgium, 1997.
[14] B. Cauberghe, P. Guillaume, P. Verboven, S. Vanlanduit, E. Parloo, On the influence of the parameter constraint on the stability of the poles and the discrimination capabilities of the stabilisation diagrams, Mech. Syst. Sig. Process. 19 (5) (2005) 989–1014.
[15] All J. Allemang, The Modal Assurance Criterion (MAC): Twenty Years of Use and Abuse, Sound Vib. (2003) 14–21.
[16] M. Kawrza, T. Furtmüller, C. Adam, Experimental and numerical modal analysis of a cross laminated timber floor system in different construction states, submitted for publication.
[17] A.W. Phillips, R.J. Allemang, Normalization of Experimental Modal Vectors to Remove Modal Vector Contamination, in: R. Allemang (Ed.), Topics in Modal Analysis II, Volume 8, Springer International Publishing, Cham, 2014, pp. 29–41.
[18] M. Kawrza, T. Furtmüller, C. Adam, R. Maderebner, Parameter identification for a point-supported cross laminated timber slab based on experimental and numerical modal analysis, Eur. J. Wood Prod. 79 (2) (2021) 317–333.